PHILOSOPHICAL TRANSACTIONS OF THE ROYAL SOCIETY B BIOLOGICAL SCIENCES

Global spectral–kinetic analysis of room temperature chlorophyll *a* fluorescence from light-harvesting antenna mutants of barley

Adam M. Gilmore, Shigeru Itoh and Govindjee

Phil. Trans. R. Soc. Lond. B 2000 **355**, 1371-1384
doi: 10.1098/rstb.2000.0699

THE ROYAL SOCIETY

doi 10.1098/rstb.2000.0699

Global spectral-kinetic analysis of room temperature chlorophyll *a* fluorescence from light-harvesting antenna mutants of barley

Adam M. Gilmore[1]*, Shigeru Itoh[2]† and Govindjee[3]

[1]*Photobioenergetics Group, Research School of Biological Sciences, Australian National University, Canberra, ACT 0200, Australia*
[2]*Department of Cell Biology, National Institute for Basic Biology, Okazaki 444, Japan*
[3]*Center for Biophysics and Computational Biology, University of Illinois at Urbana-Champaign, Urbana, IL 61801, USA*

This study presents a novel measurement, and simulation, of the time-resolved room temperature chlorophyll *a* fluorescence emission spectra from leaves of the barley wild-type and chlorophyll-*b*-deficient chlorina (*clo*) *f2* and *f104* mutants. The primary data were collected with a streak-camera-based picosecond-pulsed fluorometer that simultaneously records the spectral distribution and time dependence of the fluorescence decay. A new global spectral-kinetic analysis programme method, termed the double convolution integral (DCI) method, was developed to convolve the exciting laser pulse shape with a multimodal-distributed decay profile function that is again convolved with the spectral emission band amplitude functions. We report several key results obtained by the simultaneous spectral-kinetic acquisition and DCI methods. First, under conditions of dark-level fluorescence, when photosystem II (PS II) photochemistry is at a maximum at room temperature, both the *clo f2* and *clo f104* mutants exhibit very similar PS II spectral-decay contours as the wild-type (*wt*), with the main band centred around 685 nm. Second, dark-level fluorescence is strongly influenced beyond 700 nm by broad emission bands from PS I, and its associated antennae proteins, which exhibit much more rapid decay kinetics and strong integrated amplitudes. In particular a 705–720 nm band is present in all three samples, with a 710 nm band predominating in the *clo f2* leaves. When the PS II photochemistry becomes inhibited, maximizing the fluorescence yield, both the *clo f104* mutant and the *wt* exhibit lifetime increases for their major distribution modes from the minimal 250–500 ps range to the maximal 1500–2500 ps range for both the 685 nm and 740 nm bands. The *clo f2* mutant, however, exhibits several unique spectral-kinetic properties, attributed to its unique PS I antennae and thylakoid structure, indicating changes in both PS II fluorescence reabsorption and PS II to PS I energy transfer pathways compared to the *wt* and *clo f104*. Photoprotective energy dissipation mediated by the xanthophyll cycle pigments and the PsbS protein was uninhibited in the *clo f104* mutant but, as commonly reported in the literature, significantly inhibited in the *clo f2*; the inhibited energy dissipation is partly attributed to its thylakoid structure and PS II to PS I energy transfer properties. It is concluded that it is imperative with steady-state fluorometers, especially for *in vivo* studies of PS II efficiency or photoprotective energy dissipation, to quantify the influence of the PS I spectral emission.

Keywords: deconvolution; fluorescence lifetime distributions; L_1 robust minimization method; photosystem II; streak camera

1. INTRODUCTION

Measurements of chlorophyll *a* fluorescence, especially from photosystem II (PS II), are routinely used to gauge the status and efficiency of the photosynthetic electron transport system (Baker 1996). They provide a practical, non-intrusive measure of the various competing de-excitation pathways for the absorbed light energy, namely photochemistry, non-radiative or thermal dissipation, and fluorescence (Singhal *et al*. 1999). Dark-level fluorescence conditions, usually called F_o conditions, are defined when fluorescence is elicited by light too weak to drive photochemistry, PS II photochemistry is at a maximal rate and the primary quinone electron acceptor in PS II is oxidized; F_o conditions also assume there is no thylakoid membrane energization (see, for example, Van Kooten & Snel 1990; Govindjee 1995; Gilmore & Govindjee 1999). Measuring the dark-level fluorescence conditions is important to understand the photobiophysical light-harvesting process because F_o indicates maximal photochemical dissipation by the PS II reaction centre in the presence of minimal competition from other de-excitation pathways. When measuring F_o it is important for two reasons, especially *in vivo*, to be able to quantify any overlapping spectral-kinetic signals from photosystem I

*Author for correspondence (gilmore@rsbs.anu.edu.au).
†Present address: Department of Physics, Laboratory of Photobioenergetics, Graduate School of Science, Nagoya University, Chikusa-ku, Nagoya 4648601, Japan.

(PS I), because (i) PS I exhibits much more rapid decay kinetics than PS II (Roelofs *et al.* 1992; Schmuck & Moya 1994), and (ii) reabsorption of the shorter wavelength fluorescence from PS II decreases the amplitudes of the PS II bands relative to the longer wavelength PS I bands in leaves (Govindjee & Yang 1966; Weis 1985; Pfündel 1998). This study reports both a novel *in vivo* measurement and a global time-resolved emission spectral analysis method, known as the 'double convolution integral' or DCI method, as these are applied primarily to investigate the so-called dark-level and maximal chlorophyll *a* fluorescence yields (F_m conditions) from both PS II and PS I at room temperature.

We analysed the *in vivo* lifetimes of chlorophyll *a* fluorescence from two well-characterized light-harvesting barley mutants known as *chlorina f104* (*clo f104*) and *chlorina f2* (*clo f2*). These mutants are distinguished by unique alterations in the content and composition of the light-harvesting pigment–protein complexes associated with both PS II and PS I. The chlorophyll-*b*-less *clo f2* mutant primarily lacks the major complement of Lhcb1 and Lhcb6 proteins associated with PS II in addition to lacking the Lhca4 protein associated with PS I (Bossman *et al.* 1997; Knoetzel *et al.* 1998). The light- and temperature-sensitive *clo f104* mutant lacks a large complement of Lhcb1 in addition to lacking the 23 kD Lhca2 protein of PS I (Knoetzel & Simpson 1991; Bossman *et al.* 1997). These mutants were chosen for this study because they both exhibit strong variations in their PS I chlorophyll emission spectral amplitudes at 77 K and significant differences in their room temperature steady-state fluorescence behaviour (Simpson *et al.* 1985; Bassi *et al.* 1985). It was thus of interest to determine and characterize the probable relationships between the 77 K spectral changes due to PS I and the room temperature fluorescence parameters. More importantly it has also been reported recently that both these mutants exhibit several PS-II-related activities that do not change, as might be predicted, in conjunction with the loss of Lhcb1; namely, the light-limited quantum efficiency and fluorescence lifetimes of PS II and the well-known transthylakoid pH- and xanthophyll-cycle-dependent non-photochemical quenching (Briantais *et al.* 1996; Gilmore *et al.* 1996).

Here we report three main observations based on the simultaneous spectral-kinetic acquisition and DCI analysis of fluorescence data collected using a streak-camera spectrograph (Schiller & Alfano 1980; Tsuchiya 1984; Davis & Parigger 1992; Bühler *et al.* 1998). First, that under conditions of dark-level fluorescence both the *clo f2* and *clo f104* mutants exhibit very similar PS II spectral-decay contours to the wild-type (*wt*), with the main band centred around 685 nm. Second, that dark-level fluorescence in the *clo f2*, *clo f104* and *wt* is strongly influenced, beyond 700 nm, by broad emission bands from PS I that exhibit much more rapid decay kinetics and stronger integrated amplitudes than the main PS II band at 685 nm. Third, that *clo f2* compared with *clo f104* and *wt* exhibits different room temperature PS I emission spectral bands, unique F_o and F_m lifetime distributions and an inhibited capacity for photoprotective thermal energy dissipation. We conclude that it is imperative for *in vivo* studies of PS II photochemistry and photoprotective thermal energy dissipation using chlorophyll *a* fluorescence to quantify the influence of the prominent PS-I-related spectral emission components.

2. MATERIAL AND METHODS

(a) *Plant material and experimental details*

Seeds of *wt* barley (*Hordeum vulgare* L.) and the nuclear gene mutants *clo f2* and *clo f104* were obtained from Professor D. Simpson of the Carlsberg Research Laboratories (Copenhagen Valby, Denmark). Plants were grown in a growth chamber at 75% relative humidity under a day–night regime of 16 L : 8 D and 25 °C–20 °C. The high (HL), medium (ML) and low (LL) light growth conditions were defined as 250–270, 130–160 and 50–60 μmol photons $m^{-2} s^{-1}$, respectively.

The chlorophyll antenna sizes of PS II were determined according to the oxygen flash yield method of Chow *et al.* (1991). The PS I content was obtained from P_{700} measurements according to Schreiber *et al.* (1988). Chlorophyll determinations relevant to the antenna size estimates were performed according to the method of Porra *et al.* (1989). Quantitative analysis of the chloroplast pigments was according to the HPLC method of Gilmore & Yamamoto (1991).

(b) *Steady-state chlorophyll* a *fluorescence measurements*

Room temperature measurements of F_m and F_o were made with a PAM 101-102-103 Model chlorophyll fluorometer (Heinz-Walz, Effeltrich, Germany) equipped with a standard 650 nm excitation diode and RG-9 emission filter that cuts off all light below 690 nm, and transmits *ca.* 50% at 710 nm and *ca.* 90% >720 nm. The PAM measuring beam settings and saturating light pulse intensities for the F_m and F_o determinations were as used earlier (Gilmore *et al.* 1996).

The 77 K spectra of intact leaf pieces were performed with an SLM 8100 spectrofluorimeter (Spectronic Institute, Rochester, NY, USA) in photon counting mode. Excitation was at 435 nm (peak chlorophyll *a* absorbance) through an 8 nm slit width, and emission was monitored with a slit width of 2 nm using a monochromator slew rate of 1 nm s^{-1} and integration time of 1 s. The displayed spectra were first smoothed using the exponential algorithm by a factor of 0.4, then normalized to the peak emission channel and fit by minimizing the sum of the squared residual error (SSE) parameter,

$$\mathrm{SSE} = \sum_{i=1}^{N} (D_i - M_i)^2, \tag{1}$$

where D_i is the fluorescence intensity at wavelength coordinate λ_i, and M_i is the predicted intensity from a model comprising the sum of five free-floating Gaussian bands. Each Gaussian spectral band was defined by the following amplitude function,

$$I(\lambda)_i = \mathrm{AMP} \times \exp\left[-\frac{1}{2}\left(\frac{\lambda - \mathrm{CTR}}{\mathrm{WID}}\right)^2\right], \tag{2}$$

where AMP is the normalized maximum amplitude parameter, CTR is the mean or central mode λ parameter, and WID, the width, is the standard deviation parameter in λ units.

(c) *Time- and wavelength-resolved chlorophyll* a *fluorescence measurements*

Time-resolved emission spectra were collected in photon counting mode with a model C4334 Streakscope (Hamamatsu

Table 1. *Comparison of the antenna sizes of PS II and PS I in the leaves of wild-type* (wt), clo f2 *and* clo f104 *mutants of barley, with supporting analyses from isolated thylakoids* [a]

type	chl/area (μmol m^{-2})	PS II/chl mmol mol chl^{-1}	PS II/area (μmol m^{-2})	PS II/PS I[a,b]	P_{700}/chl (mmol mol chl^{-1})
clo f2	140 ± 3 (n = 3)	5.52 ± 0.20 (n = 4)	0.78 ± 0.04 (n = 4)	2.36	2.34
wt	248 ± 16 (n = 3)	3.21 ± 0.02 (n = 3)	0.80 ± 0.05 (n = 3)	1.87	1.72
clo f104	110 ± 4 (n = 3)	5.48 ± 0.06 (n = 5)	0.61 ± 0.02 (n = 3)	3.42	1.60

[b] In the column of PSII/PSI, data are expressed on a chl basis.

Photonics, Hamamatsu City, Japan) that was synchronized at a frequency of 1 MHz with a pulsed (650 nm) laser diode excitation source (Model PLP-20, Hamamatsu Photonics). The sample emission was dispersed with a Hamamatsu spectrograph using a grating of 50 grooves mm^{-1} and a slit width of 150 μm. Data were collected using a 2 ns time window for the dark level and a 10 ns window for the maximal level through a KC-17 filter (> 630 nm) until 150 000 shots accumulated. Trigger jitter was estimated by manufacturer's specifications at < 20 ps. The charge-coupled device (CCD) camera image (640 pixels × 480 pixels) was translated to an ASCII file. The integrated pulse profile was selected and sectioned separately from the sample image, which was binned, and integrated at a rate of five pixel columns per (65) wavelength channel(s) and three pixel rows per (159) time channel(s) prior to fitting the total of 10 335 data points. All images were normalized to unity using the photoelectron count at the peak time wavelength (t,λ) channel coordinate. The theory function and statistical analyses are defined in Appendices A and B, respectively.

For the open PS II trap conditions, primary or secondary leaves from 7–10-day-old plants were dark adapted for 30 min, then vacuum infiltrated with distilled H_2O and submersed in a front surface cuvette assembly. The temperature-controlled sample compartment (20 °C) was kept dark and the illumination by the pulsed laser diode was roughly one-half to one-fifth too low in intensity to cause spontaneous PS II trap closure. Still, data collection was interrupted every 25 000 shots to oxidize the PS II traps with 30 s of far-red illumination (Walz PAM 102, 700 nm diode, < 10 μmol photons m^{-2} s^{-1}). The F_m/F_o ratio was checked intermittently with the PAM in conjunction with the far-red illumination to ensure maximal signal stability. Measurement conditions for the closed PS II trap conditions were the same except that a blue light (440 nm centre, 10 nm band-pass, 100 μE m^{-2} s^{-1}) was used to maintain trap closure after vacuum infiltration of the leaves for 30 min with 10 μM DCMU (3-(3,4-dichlorophenyl)-1,1-dimethylurea). A background steady-state fluorescence image, collected in the absence of the pulsed laser excitation, was collected and simply subtracted from the image generated by the pulse in the presence of the background illumination.

3. RESULTS

(a) *Photosystem II and I antenna sizes, steady-state chlorophyll a fluorescence, xanthophylls and PS II energy dissipation*

Table 1 shows that the total levels of chlorophyll (a + b) per leaf area were reduced strongly in both the *clo f2* (56% of *wt*) and the medium-light-grown *clo f104* (44% of *wt*). Furthermore, the antenna size, PS II/chl, determined by the oxygen flash yield method (Chow *et al.* 1991) decreased in the mutants to a similar degree as the chlorophyll per area (table 1); in *clo f2*, both were 58% of the *wt*, whereas in *clo f104*, chlorophyll per area was 58% of *wt*, but PS II/chlorophyll was 45%; no particular significance is assigned to this small difference. The amount of PS I, estimated by the P_{700} chlorophyll absorbance measurements in thylakoids (Schreiber *et al.* 1988), appeared to increase slightly (136% of *wt*) in the *clo f2* compared to the *wt*, whereas it was slightly decreased to about 93% of *wt* in the *clo f104*. Likewise, the pattern of the PS II/PS I ratio (on a chlorophyll basis) was the same as the P_{700} content.

Figure 1 compares the changes in the photosystem chl antenna sizes (chl/PS II) to the changes in the chl a/b ratios (panel *a*), the levels of xanthophyll cycle de-epoxidation and energy dissipation (panel *b*), the room temperature chl *a* fluorescence ratios of the maximal (F_m) and dark-level F_o fluorescence (panel *c*), and the two main pools of xanthophylls namely, lutein and violaxanthin + antheraxanthin + zeaxanthin (panel *d*). Figure 1*a* compares the chlorophyll a/b ratios in *wt* and *clo f104* plants grown under three photon flux densities, namely, LL (*ca.* 50 μmol photons m^{-2} s^{-1}), ML (*ca.* 150 μmol photons m^{-2} s^{-1}) and HL (*ca.* 250 μmol photons m^{-2} s^{-1}), as well as the *clo f2* mutant plants grown under ML. The *clo f104* mutant chlorophyll a/b ratios responded sharply to the increasing photon flux density (PFD), reaching chlorophyll a/b ratios > 8. The *wt* exhibited measurable but still much smaller changes than the *clo f104* in response to the PFD levels. On the other hand, the *clo f2* mutant had virtually no chlorophyll *b* (at all the intensities, data not shown). Figure 1*c* shows the ratios of the fluorescence F_m/F_o yields under the same PFD conditions as in figure 1*a*. The *clo f104* mutant had the largest (*ca.* 8) F_m/F_o at the medium and high PFDs, but this ratio was still high (*ca.* 6) at the lowest PFD used. The *clo f2* mutant exhibited a clearly diminished F_m/F_o ratio (*ca.* 4) compared with all the other *wt* and *clo f104* sample conditions. Figure 1*b* compares the maximal levels of xanthophyll cycle de-epoxidation as measured by DPS = [zeaxanthin + antheraxanthin]/[violaxanthin + zeaxanthin + antheraxanthin] and energy dissipation as measured by the f_2 fraction calculated according to Gilmore *et al.* (1998) in thylakoids extracted from *wt* plants grown under LL (solid upside-down triangles) to *clo f104* thylakoids from LL (open upside-down triangles), ML (open triangles) and HL (open squares) grown plants. As the antenna size decreases, the DPS clearly increases as does the level of energy dissipation calculated as the f_2 fraction. However, like the F_m/F_o ratios under the high PFD, there is a slight but significant

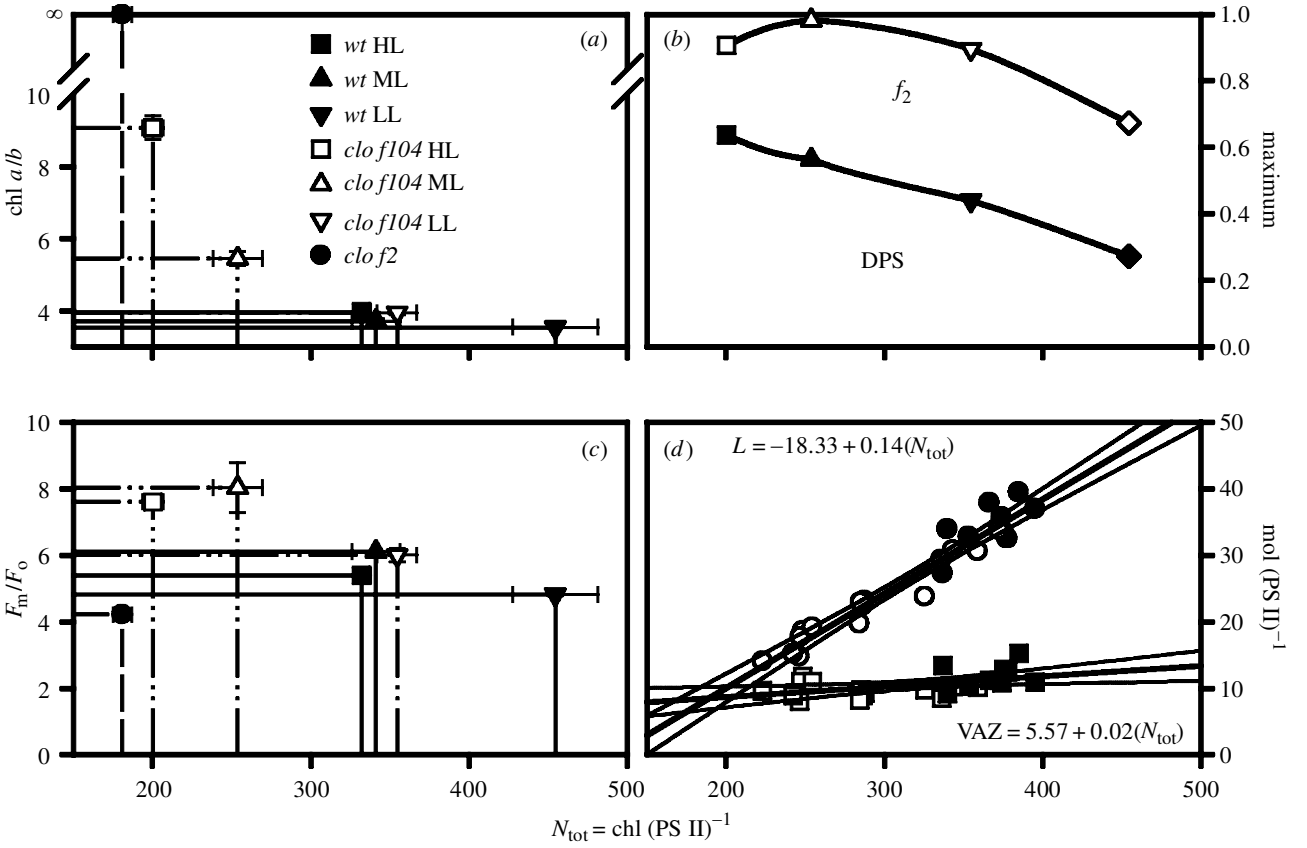

Figure 1. (*a*) Relationships between the PS II chlorophyll antenna size and the chl *a*/*b* ratio. (*b*) The xanthophyll cycle de-epoxidation state (DPS) and the level of xanthophyll-cycle-dependent energy dissipation (f_2) calculated according to Gilmore *et al.* (1998). (*c*) The ratio of the maximum (F_m) and dark (F_o) levels of chlorophyll *a* fluorescence. (*d*) Changes in the pools of lutein and the xanthophyll-cycle pigments. DPS = [zeaxanthin + antheraxanthin]/[violaxanthin + zeaxanthin + antheraxanthin]; $f_2 = -1.25(F'_m/F_m) + 1.452$; VAZ = [violaxanthin + antheraxanthin + zeaxanthin]. The data in (*a*) and (*c*) are from the same leaf samples; the drop lines in (*a*) and (*c*), respectively, show the coordination between the chlorophyll *a*/*b* and F_m/F_o and N_{tot} for the different leaf samples. The data in panels (*b*) and (*d*) represent composites from separate thylakoid preparations. The data in panel (*d*) are described with thick linear regression lines (and thin 95% confidence intervals), and equations shown ($r^2 = 0.238$ for VAZ, and $r^2 = 0.932$ for *L*); circles represent *L* for the *clo f104* (open) and *wt* (closed) and squares represent VAZ for the *clo f104* (open) and *wt* (closed).

downturn in the level of energy dissipation when comparing the high to the medium PFD conditions. Since suitably active thylakoids were not recovered from the *clo f2* in this work, we simply cite and confirm other literature that documents a clear (20–40%) decrease in the maximum levels of energy dissipation in the *clo f2* mutant, and other chlorophyll-*b*-less mutant leaves, grown under constant but moderate PFDs (Briantais 1994; Falk *et al.* 1994; Härtel & Lokstein 1995). Figure 1*d* documents the pool sizes (mol (PS II)$^{-1}$) of the xanthophyll cycle pigments (VAZ = violaxanthin + antheraxanthin + zeaxanthin) and lutein (*L*) in *wt* and *clo f104* plants grown under a range of PFDs generally inclusive of the high and low PFDs defined in the other panels of figure 1. It is clear the loss of chlorophyll *b* and decreasing PS II antenna size correlates with a loss of two-thirds of the maximum pool of L. However, consistent with the significant levels of xanthophyll-cycle-dependent energy dissipation in figure 1*b*, the levels of VAZ remained almost invariant over the range of measured growth PFDs. Elimination of the major pool of Lhcb1 in the *clo f104* reduces both L and chlorophyll *b*, does not much reduce the VAZ, but does increase the relative DPS in conjunction with the energy dissipating f_2 fraction.

Figure 2 compares the 77 K steady-state chlorophyll *a* fluorescence spectra and component bands after Gaussian deconvolution from intact leaves of the *clo f2* (figure 2*a*), *wt* (figure 2*b*) and ML-grown *clo f104* (figure 2*c*). Also shown next to the spectral panels is a tabulation of the PS II and PS I protein components in the mutants and the 77 K spectral bands that have been attributed to them. The spectra were normalized to unity at their respective emission peaks. The *clo f2* spectrum is characterized by low amplitudes of the F_{685} and F_{695} bands, from CP43 and CP47, respectively, relative to the peak emission from the F_{730} and F_{740} bands. The *clo f2* mutant is characterized by a lack of Lhcb1 and Lhcb6, and reduced Lhcb2 and Lhcb3 in PS II. The *clo f2* lacks Lhca4 from PS I and the 730 nm emission is thus attributed to the remaining Lhca1, 2 and 3 complexes. The *wt* spectrum is also characterized by low F_{685} and F_{695} amplitudes, but the *clo f2* spectrum can easily be distinguished from the *wt* since it exhibits a maximum emission peak that is broadened in width and blue-shifted by about 10 nm compared to the *wt*. The slight band resolved with a peak around 715 nm in the *wt* is tentatively attributed to PS I core complex I, CC1. The *clo f104* spectrum (figure 2*c*) is distinguished by an increased ratio of the amplitudes of F_{685} and F_{695}

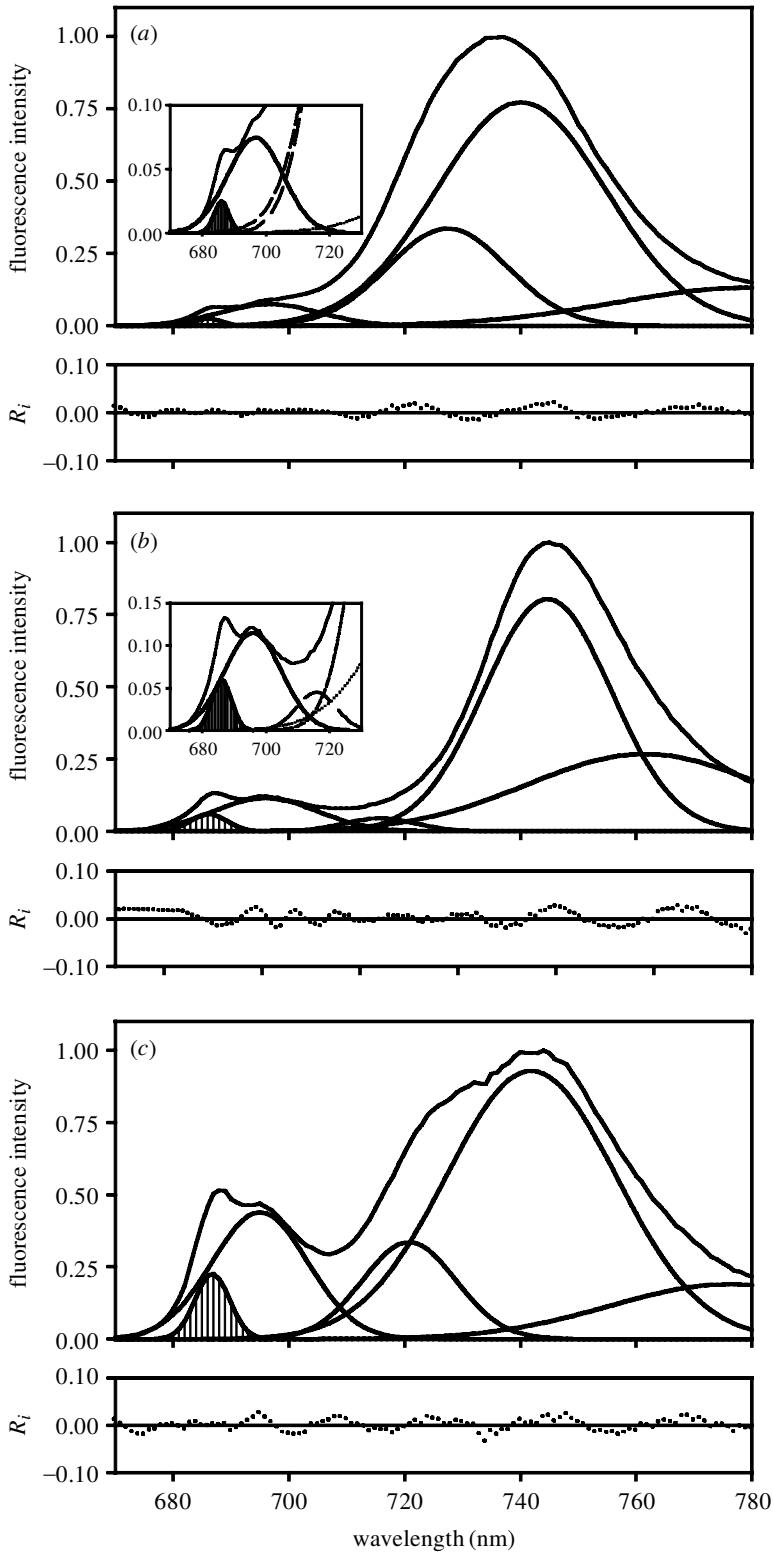

protein	level	77 K band
PS II		
Lhcb1	0	
Lhcb2	reduced	
Lhcb3	reduced	
Lhcb6	0	
PsbS	*wt*	
CP43	*wt*	685 nm
CP47	*wt*	695 nm
PS I		
Lhca1–3	*wt*	730 nm
Lhca4	0	
CC1	*wt*	720 nm

protein	level	77 K band
PS II		
Lhcb1–3	*wt*	weak 680 nm
CP43	*wt*	685 nm
CP47	*wt*	695 nm
PS I		
Lhca1–4	*wt*	740 nm
CC1	*wt*	720 nm

protein	level	77 K band
PS II		
Lhcb1	reduced	
PsbS	*wt*	
CP43	*wt*	685 nm
CP47	*wt*	695 nm
PS I		
Lhca1	*wt*	740 nm
Lhca2	reduced	
Lhca4	*wt*	
CC1	*wt*	720 nm

Figure 2. Fluorescence spectral emission profiles, and Gaussian deconvolution of the emission band components, for barley *chlorina f2* (*clo f2*) (*a*), wild-type (*wt*) (*b*), and *chlorina f104* (*clo f104*) (*c*) mutant leaves at liquid nitrogen temperature (77 K) (left panels). Each spectrum was normalized to the peak emission and fitted with five free-floating Gaussians. The insets in (*a*) and (*b*) focus on the spectral region associated with short-wavelength antennae emissions, mainly from the PS II core. The subplots, below the main panels, represent the residual errors (R_i) corresponding to the Gaussian model. The data for the tables (right panels) were adapted from Bossman *et al.* (1997) for (*a*) and (*b*), and Knoetzel & Simpson (1991) for (*c*).

relative to F_{740}, compared to the *wt* and *clo f2*. Further, the *clo f104* spectrum displays a prominent band centred around 720 nm, certainly attributed to CC1. The *clo f104* PS II protein composition is distinguished by a strong reduction in Lhcb1 while the PS I protein composition denotes reduced levels of Lhca2 and 3 (also known as LHC I-680). Although some 77 K studies report a small 680 nm band arising from Lhcb1, 2 and 3 (Simpson *et al.*

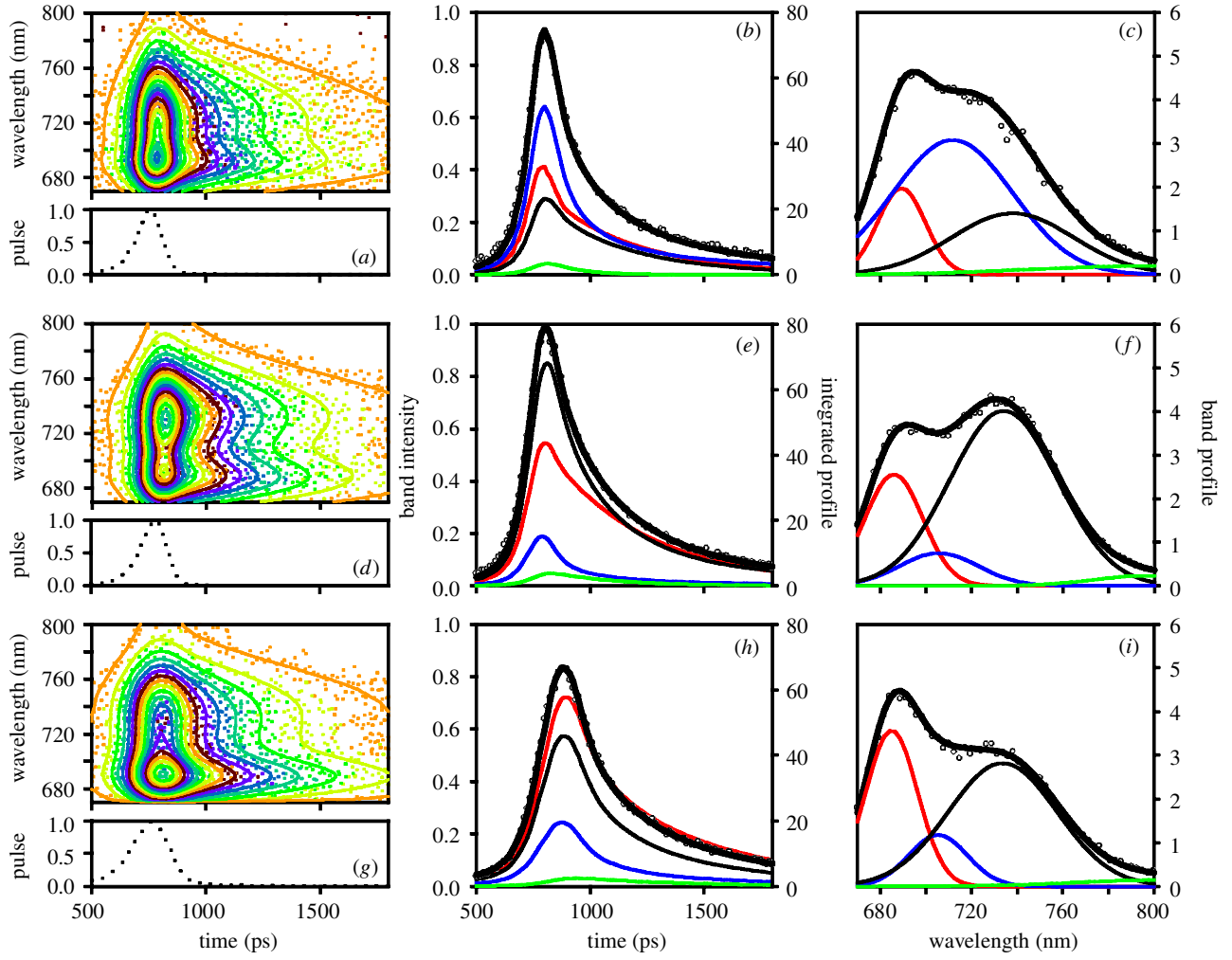

Figure 3. Time and wavelength resolved fluorescence spectra and their deconvolved components for barley *chlorina f2* (*clo f2*) ((*a*), (*b*) and (*c*)), wild-type (*wt*) ((*d*), (*e*) and (*f*)) and *chlorina f104* (*clo f104*) ((*g*), (*h*) and (*i*)) mutant leaves at room temperature measured with the streak-camera spectrograph. The subplots, under panels (*a*), (*d*) and (*g*) depict the instrument pulse–response profiles that were convolved with the respective model decay functions (see Appendix A) to yield the model curves (lines). The fit was determined using the robust L_1 method (see Appendix B) for minimizing the absolute deviations. Panels (*b*), (*e*) and (*h*) depict the integral intensity profiles (right ordinate) for the complete spectral integral (680 to 800 nm) of the model (thickest line) and data points (open circles); the left ordinate refers to each of the four main component emission band amplitude profiles (red, blue, black and green) linked to the centre of gravity wavelength of the respective emission bands in panels (*c*), (*f*) and (*i*). Panels (*c*), (*f*) and (*i*) depict the Gaussian band profiles for the time integral (peak plus five subsequent time channels) of the model (thickest line), actual data points (open circles) and each of the four component emission bands (red, blue, black and green).

1985; Falbel *et al*. 1994; Krugh & Miles 1995), this band was not resolved in any samples in this study. Perhaps, it is hidden in the short-wave side of the F_{685} band in the *wt* assuming it may be narrower than this fit indicates. Further work may answer this question.

(b) *Time-resolved chlorophyll* a *fluorescence emission spectra of the barley* clo f2, wt *and* clo f104 *leaves*

Figure 3 compares the contoured top-views and the deconvolved spectral-kinetic components from the time-resolved dark-level chlorophyll *a* fluorescence spectra and L_1 model fits for the *clo f2* (figure 3*a–c*), *wt* (figure 3*d–f*) and *clo f104* (figure 3*g–i*) barley leaves at room temperature. The instrument pulse-response profiles of the streak-camera spectrograph are shown as subpanels at the base of figure 3*a*,*d*,*g*. In contrast to the large differences in the PS II antenna sizes described in § 3(a) (table 1 and figure 1), each of fluorescence spectra exhibit similar overall kinetics in the contoured region around 685 nm; this is one of the two major observable peaks in all leaves at room temperature. The normalized pulse-induced fluorescence rises and decays around 685 nm fit similarly within the same time-frame for each sample in figure 3. Consistent with the 77 K spectra shown in figure 2, the *clo f2* spectral decay (figure 3*a*) showed an overall blue-shift in its far-red region compared to the *wt* (figure 3*d*), which showed its peak emission as a broad contour around 740 nm. Also consistent with the 77 K steady-state spectra in figure 1, the *clo f104* (figure 3*g*) showed a strongly diminished intensity of its major far-red contour (of its 740–685 ratio), compared with the 685 nm contour, as compared with the *wt* (figure 3*d*).

The spectral-kinetic profiles are compared in side views in figure 3*b*,*e*,*h* and represent the kinetics of the

intensity at the centre of gravity wavelength for the different fluorescence bands illustrated in figure 3*c*,*f*,*i*, which themselves represent the spectra in the front view. The thick lines in the profile plots represent the integrated model and the open circles represent the integral data points. The front views are the integrated intensity of the peak and five subsequent time channels (integral = 74 ps). The band intensity profiles for the *clo f2* (figure 3*b*, kinetics, and 3*c*, spectra) illustrate three major bands, namely the F_{685} (red in the figure), the F_{710} (blue), and the F_{740} (black). The F_{685} band, most of which is from PS II, decays with comparable kinetics to the F_{740} band while the F_{710} band decays the fastest. The large F_{710} amplitude clearly dominates the decay spectrum in figure 3*a*–*c* and determines the gradually sloping far-red spectral region that is clearly blue-shifted when compared to the *wt* (figure 3*d*–*f*). A broad but minor far-red band (centred at 796 nm) was included to improve the fit in all three images; it exhibited similar decay kinetics as the F_{740} band and was interpreted as a satellite band. It is well known that chlorophyll *a* fluorescence has a major electronic band followed by a satellite band. It is therefore reasonable to assume that this band is a satellite band of chlorophyll fluorescing in the long-wave region (e.g. an F_{740} satellite band), just as a satellite band is expected in the 740 nm region for F_{685}.

The *wt* band intensity profile (figure 3*e*,*f*) is initially dominated by the F_{740} band (black in the figure) that decays more rapidly than the F_{685} band (red) and crosses below it, around the 1200 ps mark; the F_{705} band (blue) has a low amplitude and has the most rapid overall decay. In contrast to the *wt*, the *clo f104* spectrum is dominated at all times by the F_{685} band (red); the band intensity profile (figure 3*h*,*i*) shows the F_{740} band (black) does not exceed 75% of F_{685} at the peak of the pulse and decays more rapidly than F_{685} following the pulse peak. The minor F_{710} band showed almost identical decay kinetics as F_{705} in the *wt*.

The *clo f104* band spectral profile (figure 3*g*–*i*) shows that the integrated intensity of F_{740} is clearly depressed compared with the *wt*, while the kinetics and spectrum of the F_{705} band (blue in the figure) is quite similar. The minor far-red band showed almost identical decay kinetics as F_{740} in the *wt* above. A scatter band (τCTR $\approx$ 0.00 ps) centred at 650 nm was also included in the model fits for all samples to account for a slight overlap of the diode laser tail emission with the sample—but because the integrated intensity of this band was very low it had little statistical and no visual impact on the data or model presentation, and hence is not illustrated in figure 3.

(c) *Model decay distribution profiles and fitting parameters*

Figure 4 compares the multimodal distribution profiles that represent the model decay functions for the dark-level (F_o) and maximal (F_m) fluorescence conditions for *clo f2* (figure 4*a*,*b*), *wt* (figure 4*c*,*d*) and *clo f104* (figure 4*e*,*f*). The multimodal-distributed decay functions shown in the major panels for the dark-level images are expressed as the lifetime-weighted pre-exponential amplitude factor, $\alpha\tau(\tau)$: this is to emphasize those components most heavily weighted in intensity. The inset figures show the distributed pre-exponential amplitude factor $\alpha(\tau)$; they illustrate significant contributions of component amplitudes with faster fluorescence lifetimes (< 1000 ps). Figure 4 shows that the major and most heavily weighted mode of fluorescence lifetime distribution for F_{685} is *ca.* 400–500 ps in all three samples with the traps open. The insets in figure 4*a*,*c*,*e* also show that for the open trap conditions the lifetime distributions were clearly multimodal for the F_{685} bands in all three samples; each exhibited one tailed modes centred below 100 ps in addition to the more heavily weighted *ca.* 400–500 ps modes; it is possible that the faster component is the PS I F_{685}, and the latter the PS II F_{685}. The F_{705} in the *wt* and *clo f104* was clearly lower in amplitude compared with F_{710} in the *clo f2*. The *clo f2* open trap conditions were characterized by the very prominent single and short mode for F_{710} < 100 ps, whereas F_{740} was bimodal and very similar to F_{685} in both modes, again suggesting its origin in both PS I and PS II. Compared to the *clo f2* (figure 4*a*) the *wt* (figure 4*b*) and *clo f104* (figure 4*c*) exhibited similar major modes around 250–350 ps for F_{740}.

The *clo f2* closed trap conditions were characterized by extremely broad major modes for F_{685} and F_{740} with amplitudes peaking in the 1200–1500 ps range and long tails extending to > 5 ns; both the major F_{685} and F_{740} modes integrated to lifetimes > 2200 ps. The anomalous F_{685} and F_{740} bandwidths and attenuated centre modes were consistent with decay kinetics resolved by phase-modulation fluorometry for the *clo f2* under both minimal and maximal PS II fluorescence conditions (data not shown). Consistent with the anomalous F_{685} and F_{740} distributions a unique and relatively minor narrow mode was resolved in *clo f2* for the F_{710} band around 500 ps under the maximal fluorescence conditions.

Compared with the anomalous *clo f2* (figure 4*b*), the *wt* (figure 4*d*) and *clo f104* (figure 4*f*) exhibited remarkably similar major modes around 1900–2000 ps for both F_{685} and F_{740}. The major F_{740} modes were generally a few hundred picoseconds faster than F_{685} in both the *wt* and *clo f104*. The major F_{740} mode in the *clo f104* exhibited a reduced integral amplitude compared to the *wt*. The F_{740} bands of the *wt* and *clo f104* also exhibited broad minor modes in the sub 1000 ps range—likewise, a similar minor mode was observed for F_{685} in the *clo f104*.

(d) *Residual error analyses for the χ^2_v and L_1-robust minimization methods*

Table 2 shows the results of the Runs tests, the Durbin–Watson *d*-statistic tests and the second χ^2-tests used to comparatively evaluate the dark-level image fits obtained from the χ^2_v and L_1 methods. The Runs tests compare the expected and observed number of runs (consecutive residual signs between sign changes) as a global average for all the time-series (each λ channel) by computing the standard normal variates $\mathcal{Z}_{tf}$, indicating too few, and $\mathcal{Z}_{tm}$, indicating too many runs, per time-series. For each image and material it was clear the Runs tests indicated the L_1 method yielded more uniformly randomized residual signs when compared to the χ^2_v method. This was evident from the reduced mean and standard deviation values for both the standard normal variates. The $\pm\sigma$-values clearly overlapped the natural mean (= 2) of the *d*-statistic distribution in each sample to indicate that the data

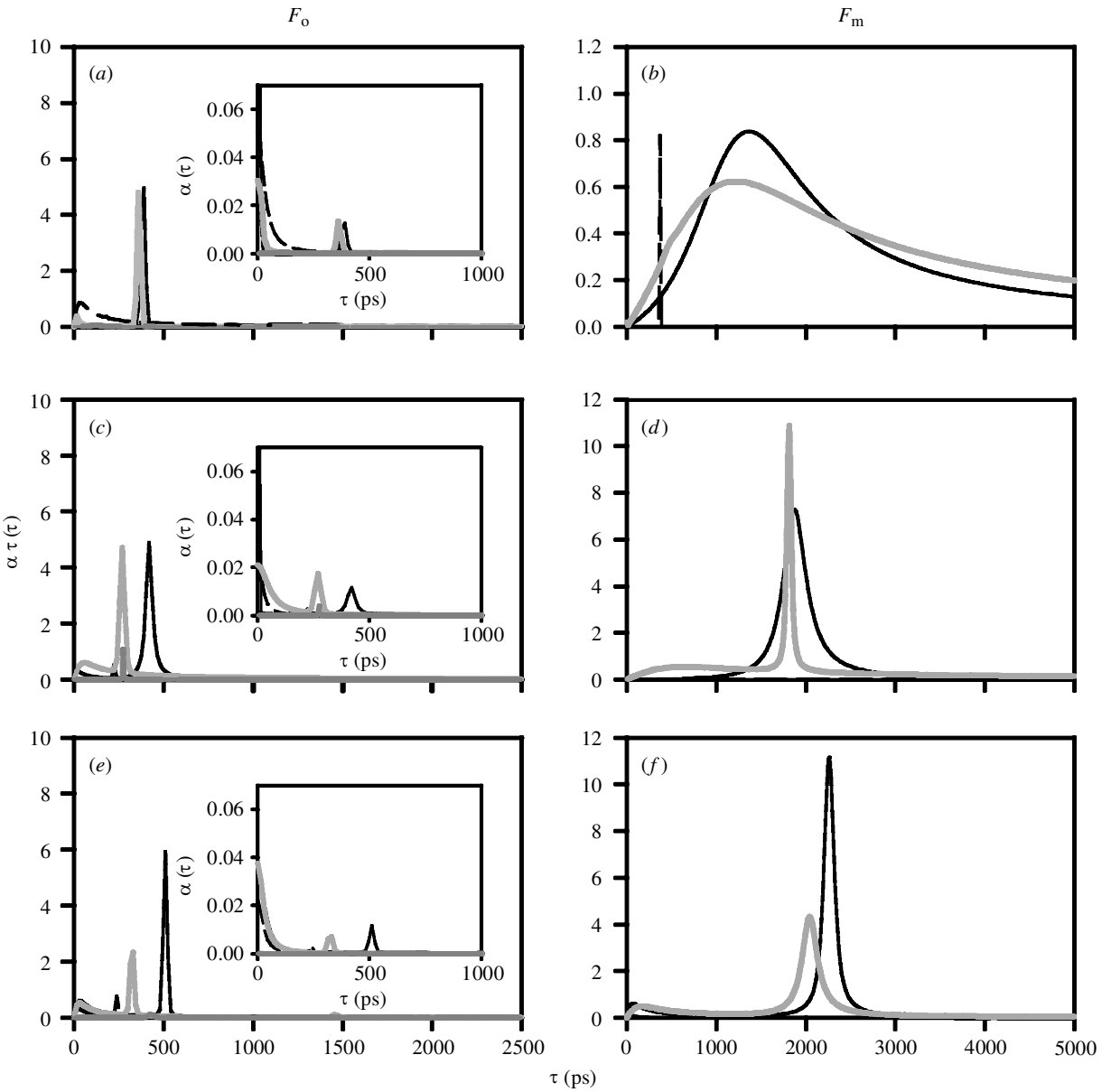

Figure 4. Chlorophyll *a* fluorescence lifetime distribution profiles corresponding to the spectral components for the barley *chlorina f2* (*clo f2*) (*a*,*b*), wild-type (*wt*) (*c*,*d*) and *chlorina f104* (*clo f104*) (*e*,*f*) leaves. Panels (*a*), (*c*) and (*e*) represent the dark-level fluorescence, F_o, and depict the lifetime-weighted distribution of the pre-exponential amplitude factor $\alpha\tau(\tau)$ for the respective spectral bands, whereas, the insets in each panel depict the distribution of the pre-exponential amplitude factor $\alpha(\tau)$. Panels (*b*), (*d*) and (*f*) represent the maximal fluorescence, F_m, models and depict the lifetime-weighted distribution of the pre-exponential amplitude factor ($\alpha\tau(\tau)$) for the respective spectral bands. The respective bands coloured in figure 3 as red, blue, black and green are denoted as black, dashed, grey and dark grey in figure 4. The L_1 statistics (see Appendix B) for the dark-level fluorescence images (*a*,*c*,*e*) are listed in table 2 while the L_1 statistics for the maximal-level fluorescence images for (*b*), (*d*) and (*f*) are 146, 165 and 122, respectively.

exhibit no extreme systematic serial trends. The mean value was closer to 2 in the *clo f2* and *wt* L_1 method fits than in the corresponding χ^2_v method fits, but the *d*-statistic mean did not indicate an improved L_1 method fit in the *clo f104*. The binned histogram analyses of the residual errors from both the χ^2_v and L_1 methods yielded the second χ^2-statistics. The analyses were designed to test the hypothesis that the residual error distribution was normal, as assumed for the χ^2_v method, as opposed to a Laplace distribution with a more peaked shape and more heavily populated symmetrical tails as assumed for the L_1 method. It was clear that for all three samples the fit of the residual error histogram to the error function converged on the Laplace shape = 2 (see footnote to table 2) for both the χ^2_v and L_1 methods. It was also clear that in each image the L_1 method led to the lowest and most significant second χ^2-statistic.

4. DISCUSSION

(a) *Time-resolved emission spectra of barley* chlorina *mutants*

The most striking features of the images in this study were the large variations in the PS-I-associated dark-level fluorescence spectral decay components in the *clo f2* and *clo f104* mutants compared to the *wt*. It is clear that the

Table 2. *Comparative statistical characterization of the dark-level fluorescence images from the* clo f2, wt *and* clo f104 *leaves.*

(All statistical parameters are defined in Appendix B, including the standard normal variates for the Runs test, the Durbin–Watson *d*-statistic, the second chi-squared statistic (χ^2), the reduced chi-squared (χ^2_v), and the robust L_1 methods.)

			$\lvert Z_{tf}\rvert$		$\lvert Z_{tm}\rvert$		*d*		second χ^2 [a]	
leaf	χ^2_v	L_1	χ^2_v	L_1	χ^2_v	L_1	χ^2_v	L_1	χ^2_v	L_1
clo f2	0.0238	173	0.963 ± 0.740	0.897 ± 0.662	1.088 ± 0.773	0.983 ± 0.701	1.873 ± 0.260	1.910 ± 0.261	1.040	0.778
wt	0.0099	136	1.147 ± 0.823	0.889 ± 0.685	1.292 ± 0.846	0.989 ± 0.709	1.872 ± 0.215	1.896 ± 0.208	0.885	0.646
clo f104	0.0074	137	1.541 ± 1.013	1.323 ± 0.817	1.652 ± 1.061	1.418 ± 0.872	1.856 ± 0.233	1.837 ± 0.229	0.834	0.707

[a]In each case the best fit for the second χ^2-statistic converged on a shape parameter = 2 indicating Laplace, as opposed to normal, residual error distributions.

steady-state spectral variations observed at 77 K for the mutant leaves (Simpson *et al.* 1985; Knoetzel *et al.* 1997; this study) are strongly echoed in the room temperature spectral analysis. It is also evident that self-absorption of the PS II fluorescence in the leaves at room temperatures increased the amplitudes of the far-red bands, which are mostly from PS I, relative to the F_{685} band. We conclude that reabsorption thus plays a major role in determining the amplitudes of the room temperature fluorescence components as it has been established at 77 K (Govindjee & Yang 1966; Weis 1985).

The *clo f2* is of particular interest because of its anomalous spectral-kinetic properties compared to the *clo f104* and *wt*. Lack of Lhca4 in *clo f2*, as described by Knoetzel *et al.* (1998), accompanies the far-red spectral changes. Melkozernov *et al.* (1998) have quantified the fluorescence lifetime behaviour of the Lhca4 and Lhca1 subunits *in vitro* and also documented changes in energy transfer and decay components that are attributable to changed pigment–protein interactions between the monomers compared with the Lhca4–Lhca1 heterodimer that comprises the LHC I-730 complex.

Both the dark and maximal fluorescence levels of the *clo f2* are considerably anomalous compared with *wt* and *clo f104*, which are actually quite similar aside from the relative amplitudes of the F_{740} bands. The *clo f2* anomalies, compared to the *wt* and *clo f104*, primarily include (i) the blue-shifted broad emission spectrum, (ii) the unique decay distribution at F_m for the F_{710}, and (iii) the broadened, attenuated F_{685} and F_{740} distribution modes at F_m. It is clear that the F_{710} band originates mainly from PS I and is likely to be of a similar nature to the PS I band first observed by Lavorel (1963) at 712–718 nm. We conclude the spectral-kinetic behaviour of *clo f2* is complex and strongly influenced by altered energy transfer pathways and reabsorption patterns between PS II and PS I. The observed changes must be partly attributed to changed absorption–emission overlap integrals and reabsorption profiles for the F_{685} and F_{710} bands, and the F_{685} (and/or F_{710}) and F_{740} bands, respectively.

The anomalous *in vivo* PS II fluorescence lifetimes in *clo f2* clearly are physically related to the well-known Mg^{2+} effects on isolated *clo f2* thylakoids, with respect to stacking and PS II versus PS I emission (Bassi *et al.* 1985). Isolated *clo f2* thylakoids, compared to the *wt* and *clo f104*, are quite labile with respect to stacking and require high Mg^{2+} and chelating agents to induce and retain stacking *in vitro*. Without the Mg^{2+} and chelation treatment there is a strong attenuation in the lifetime centre of the 2.0 ns (F_{685}) PS II distribution mode that results in a strongly inhibited F_v/F_m and inhibited xanthophyll-cycle-dependent energy dissipation (Gilmore *et al.* 1996). The well-documented Mg^{2+}-sensitive PS II quenching by PS I primarily affects F_m and not F_o (Krause *et al.* 1983). To explain the *in vivo* results of this study, in light of the *clo f2* phenotype, we hypothesize that PS II units that structurally interface with PS I units in the outer, poorly formed granal stacks in the leaves may exhibit strong quenching by energy transfer to PS I that shortens the F_m fluorescence lifetimes. Thus, the broadening and attenuation of the F_m lifetime distributions in the *clo f2* (figure 4*b*) may indicate the mixed emission from PS II units in the outer granal stacks (in excitonic contact with PS I) and weakly quenched units in the inner granal regions, disconnected from PS I, and those PS II units in intermediate locations.

Another interesting and important result of this study is the similarity of the PS-II-associated spectral-kinetic contours of the 685 nm band at F_o for the *clo f2*, *clo f104* and *wt*. It is well established, and documented in table 1, that both the *clo f2* and the *clo f104* grown under the prescribed conditions exhibit major decreases in their peripheral PS II antennae components, primarily due to reduced Lhcb1 levels. However, as shown previously these changes do not directly correlate with the changes in the fluorescence lifetimes of the PS II 685 nm band under the F_o conditions (Briantais *et al.* 1996; Gilmore *et al.* 1996). Much earlier, Haehnel *et al.* (1982) also reported similar PS II decay kinetics at F_o for intermittent-light-grown pea chloroplasts depleted of Lhcb1 as for normal pea chloroplasts. The preponderance of data indicate that the peripheral antennae chlorophylls of the Lhcbs 1–3 are not absolutely equilibrated kinetically with inner-core antennae chlorophyll *a* molecules. It is clear that the fluorescence lifetimes are not linearly determined by the number of total chlorophyll *a*s in the PS II unit at either the F_o or F_m levels. Similarly, it appears that the PS I antenna mutations in the *chlorina* mutants have much more significant influence on the amplitudes and emission spectral energy levels than on the absolute decay kinetics. This can be explained by recognizing that loss of chlorophyll *b* destabilizes certain Lhcs of PS I such that they decompose, forcing the remaining Lhcs to reorganize and yield new heterocomplexes with altered geometric arrangements and energy transfer connections, and hence changed emission amplitudes and energy levels.

With respect to PS II, an absolute linear relationship between τ and $N = \text{chlorophyll } a \text{ (PS II)}^{-1}$ is, in fact, predicted only if one assumes that each chlorophyll of PS II has an equal probability for exciton residence during a random walk of the Frenkel exciton through the entire chlorophyll matrix of the photosystem (Pearlstein 1982). This overly simplified assumption would require that each chlorophyll site in the lattice is uniformly spaced from, and isoenergetic with, its neighbour sites. Although it still remains to be determined, the lack of exciton equilibration between the Lhcb pool in the peripheral antennae and the PS II core-inner antennae is probably primarily due to entropic (structural) features as opposed to spectral (energetic) features (Holcomb & Knox 1996; Gilmore & Govindjee 1999). This is proposed since the chlorophyll *a* energy levels of the Lhcbs are believed to be nearly isoenergetic with the main chlorophyll *a* pool in the PS II core antenna (Roelofs *et al.* 1992).

Furthermore, with respect to structural features of the antennae, the xanthophyll-cycle-dependent non-photochemical quenching activity, associated with PS II, is probably conserved in these mutants, especially *clo f104* (Gilmore *et al.* 1996, 1998), because they each contain wild-type levels of the PsbS protein in the PS II inner-core antennae (Bossman *et al.* 1997). The PsbS protein has recently been established as a requisite for the conformational changes involved in xanthophyll-cycle-dependent non-photochemical quenching (Li *et al.* 2000). Inhibition of xanthophyll-cycle-dependent energy dissipation in the *clo f2* or other completely chlorophyll-*b*-less mutants or etiolated systems might be expected to be strongly influenced by the PS-I-associated anomalies pointed out earlier. In fact these changes could alter the absorption–emission overlap integrals between PS II and PS I and or the fluorescence reabsorption patterns to influence directly and quench the emission from PS II. Xanthophyll-cycle-dependent attenuation of the F_m fluorescence yield would thus be inhibited by the competing de-excitation rate process of PS II energy transfer to PS I.

It is self-evident that room temperature fluorescence measurements of the *clo f104* and *clo f2* mutants using emission filters such as the Schott RG-9 filter, which cuts off 100% below 690 nm and 50% at 710 nm, entirely eliminates the majority of the longest lifetime component from PS II, namely the 685 nm band. These cut-off filters would thus be expected to have a significant influence on the fluorescence intensity readings, since the main and slowest decaying PS II band (F_{685}) is directly and strongly obscured. Therefore, it is concluded that the differences observed for the PS II efficiency and room temperature chlorophyll *a* fluorescence intensity ratios with the PAM between the *clo f2*, *clo f104* and *wt* (see, for example, Simpson *et al.* 1985; Gilmore *et al.* 1996) are strongly influenced by the PS I contributions to the F_m and F_o fluorescence intensity readings. This conclusion is consistent with several other reports by Pfündel (1998), Genty *et al.* (1990), Adams *et al.* (1990) and Schmuck & Moya (1994). A recommended way to measure and account for PS-I-related emission with a commercial PAM chlorophyll fluorometer is to use a blue or green light-emitting diode for excitation in combination with either a band-pass filter ($F = 685$ nm) or a long-pass filter ($F > 660$ nm) to capture the respective PS II or total leaf chlorophyll emission.

(b) *Streak-camera spectrograph and double convolution integral method*

This study reports the first use of a new global data analysis method designed to facilitate a complete three-dimensional, distribution-based simulation of the time-resolved emission spectrum from a time-correlated single photon counting instrument. The double convolution integral (DCI) method, developed herein, can be compared to both the conventional decay-associated spectra (DAS), and related time-resolved emission spectra (TRES) methods (Hodges & Moya 1986; Holzwarth 1988; Knutson 1992; Roelofs *et al.* 1992; Hungerford & Birch 1996). The DAS fitting method minimizes the residual error sum by searching for amplitude and decay parameters to simulate each wavelength channel individually based on the assumption there is a physical relationship between adjacent wavelength channels in the form of variable amplitude fractions components with the same fluorescence lifetimes. The linked lifetime amplitudes define the spectral shape of a component, and the lifetime components are usually assumed to be discrete, as opposed to distributed parameters. The DCI method, in contrast to the DAS method, works under the assumption that Gaussian spectral bands determine the relative distributed amplitudes of the lifetime components that may also exhibit distributed and possibly multimodal kinetic features. The DCI method is particularly suited for simultaneously acquired spectral-kinetic data, as obtained with the streak-camera spectrograph, and does not require independent determination of the steady-state emission spectrum. The DAS method usually involves calculating so-called 'local' χ^2_v-statistics for each wavelength channel that are then used to generate a composite global χ^2_v-statistic. The DCI method generates a single global statistic that takes into account each and every (t,λ) channel coordinate simultaneously. The DCI method significantly reduces the number of free-fitting parameters compared to the DAS and TRES methods, hence facilitating a more statistically significant solution.

With respect to the data in this paper it was clear that the χ^2_v method did not yield the most reproducible or statistically significant results. In fact, the resultant residual error distributions from the χ^2_v method were decidedly Laplace-like in shape. The L_1 method led to consistently more significant randomization of the residual error signs in each time-series and in most cases similar or better autocorrelation scores based on the Durbin–Watson, *d*-statistic. The use of the L_1 method is statistically justified for the DCI method because the L_1 method is designed to resolve smaller amplitude signals with low error amplitudes that may be convolved with larger amplitude signals with respectively larger error amplitudes, because the former are not weighted as heavily. In fact, robust fitting is specially suited for data sets where the *y*-axis (amplitude) variable spans more than four log divisions, as is common with time-correlated single photon counting (Rundel 1991). We interpret the improved significance of the L_1 method to imply that

intrinsic systematic errors, possibly associated with the various instrument response convolutions and particularly the CCD camera, lead to a Laplace error distribution for the photoelectron counts recorded by the instrument (Schiller & Alfano 1980; Campillo & Shapiro 1983; Tsuchiya 1984; Davis & Parigger 1992).

We thank the National Institute for Basic Biology (NIBB) for a Visiting Scientist Award (A.M.G.), Professor N. Murata and his laboratory staff for assistance in growing plants and providing experimental and financial support, and The Australian Department of Industry, Science and Tourism, grant 97/0638 and 97/0709, for travel funds and financial support of the initial phase of the project. Special thanks are due to Dr W. S. Chow of the Australian National University (ANU) Research School of Biological Sciences (RSBS) Photobioenergetics (PBE) group for performing the photosynthetic unit size measurements. The present work was started at the University of Illinois at Urbana where A.M.G. worked on the Integrative Photosynthesis Grant. Govindjee was supported by an ANU RSBS Visiting Fellowship. S.I. was supported by Grants-in-Aid on Priority-Area-Research (molecular biometallics and single electron transfer devices) from the Ministry of Education, Science, Sports and Culture, Japan.

APPENDIX A. THEORY FUNCTION FOR THE TIME- AND WAVELENGTH-RESOLVED FLUORESCENCE ANALYSIS

The time- and spectral-resolved fluorescence model assumes that the room-temperature chlorophyll *a* fluorescence decay from the higher plant photosynthetic apparatus comprises continuous, multimodal distributions of decay components for the following three reasons:

(i) proteins exhibit conformational dynamics that may influence protein-bound fluorophores (Alcala *et al.* 1987; Frauenfelder *et al.* 1988);
(ii) the photosynthetic apparatus is heterogenous in pigment–protein composition (antennae and reaction centres);
(iii) the physiological state of the sample may fluctuate slightly during the acquisition with respect to reaction centre trap closure among other biochemical changes.

The model derivation also assumes that the total chlorophyll *a* fluorescence emission comprises a number of distinct emission bands (Govindjee 1995) that arise from particular pigment–protein complexes (antennae and reaction centres of PS I and PS II) and are almost purely Gaussian in nature with respect to their spectral wavelength energy distribution (Lin & Knox 1988; Mimuro *et al.* 1989; Yamazaki *et al.* 1984).

Individual model fluorescence lifetime decay functions were assigned to each spectral wavelength band$_{i\ldots n}$, according to the following generalized function,

$$F(t-t')_i = \begin{cases} \int_0^\infty \alpha(\tau)_i \exp[-(t-t')/\tau]\,\mathrm{d}\tau; & t > t' \\ 0; & t \leqslant t' \end{cases}, \quad \text{(A1)}$$

where the fluorescence intensity at any time $t-t'$ is determined by evaluating the integral when $t > t'$ but is 0 when $t \leqslant t'$. In equation (A1), $\alpha(\tau)_i$ represents the continuous multimodal distribution of the pre-exponential amplitude factor as a function of fluorescence lifetime, τ; $\alpha(\tau)_i$ is determined as the sum of varying contributions of the Gaussian–Lorentzian sum function defined later. In the following analyses, the continuous $\alpha(\tau)_i$ integral shown above was approximated as a discrete distribution comprising 500 channels (15 ps channel^{-1}) over the definite integral (0–15 ns); it was found that for these samples the fits obtained to $\alpha(\tau)_i$ were uninfluenced by the specified bounds. The resulting integral decay function $F(t-t')_i$ was then numerically convolved with the instrument response profile, plus a time-axis shift, $L(t'-t_{\mathrm{shift}})$ to yield the following convolution integral that predicts the normalized intensity at any time t for each band$_{i\ldots n}$, i.e.

$$I(t)_i = \int_{-\infty}^{t} L(t'-t_{\mathrm{shift}}) \times F(t-t')_i\,\mathrm{d}t, \quad \text{(A2)}$$

defined more compactly as

$$I(t)_i = L(t-t_{\mathrm{shift}}) \otimes F(t)_i. \quad \text{(A3)}$$

The normalized, continuous distribution of the intensity as a function of wavelength, λ, for each band$_{i\ldots n}$, was defined by a Gaussian spectral line shape with the amplitude function (see equation (2)); the CTR and WID parameters were globally linked through all time channels for each band$_{i\ldots n}$. It follows that in order to evaluate the intensity at any point in time, t, and at any wavelength, λ, $I(t)_i$ was convolved with $I(\lambda)_i$ by multiplying the normalized Gaussian AMP factor by $I(t)_i$ to yield the double convolution integral,

$$I(t,\lambda)_i = I(t)_t \otimes I(\lambda)_i \quad \text{(A4)}$$

for each band$_{i\ldots n}$. The final simulated image was defined simply as

$$T(t,\lambda) = \mathrm{OFFSET}(t,\lambda) + \sum_{i=1}^{N} I(t,\lambda)_i, \quad \text{(A5)}$$

which represents the summed contributions of $I(t,\lambda)_{i\ldots n}$, for all bands in the t versus λ grid, plus a vertical OFFSET(t,λ) that was a global parameter for every (t,λ) coordinate to simulate and account for uniform background noise contributions.

The integrated distribution of the pre-exponential amplitude factor, α, of the fluorescence lifetime, τ, is defined as the $\alpha(\tau)_i$ component of $F(t-t')_i$ in equation (A1) and was determined in our model fits by using varying summed combinations, the Gaussian–Lorentzian sum distribution function (Rundel 1991). This function sums equal full-width at half-maximum Gaussian and Lorentzian distributions and comprises four changing parameters, namely, the WID (full-width at half-maximum amplitude), the peak (modal) amplitude (AMP), the centre or mode (CTR), and the shape (SHAPE). The WID must be > 0, and the SHAPE can only vary between 0 and 1, where SHAPE = 0 is a pure Lorentzian and SHAPE = 1 is a pure Gaussian.

APPENDIX B. STATISTICAL ANALYSIS OF THE TIME-RESOLVED FLUORESCENCE SPECTRAL IMAGES

(a) χ^2 method

The images were simulated and analysed using Microsoft[1] Excel 97 and Visual Basic Macro programming. The residual errors $R_i = D_i - M_i$ were weighted assuming a Poisson distribution of errors at each (t,λ) coordinate that can be approximated, given a sufficient number of counts, by a Gaussian distribution. We recall that D_i is the fluorescence intensity at time-wavelength coordinate $(t,\lambda)_i$ and M_i is the predicted intensity for the same $(t,\lambda)_i$ coordinate. The residual weighting is approximated as the standard deviation or the square root of the intensity value at each $(t,\lambda)_i$ coordinate as $\sigma \cong \sqrt{M_i}$. The least-squares model fits were evaluated based on the randomness of the weighted residuals and by comparing the reduced χ^2-statistic calculated according to Bevington (1969) as

$$\chi^2_v = \frac{1}{N - m - 1} \sum_{i=1}^{N} \left(\frac{(D_i - M_i)^2}{M_i} \right), \tag{B1}$$

where $N = 10\,335$ is the number of (t,λ) coordinate channels, m is the number of dynamic model-fitting parameters, $(D_i - M_i)^2$ represents the squared residual error at each $(t,\lambda)_i$.

(b) L_1 method for robust minimization of the absolute deviations

The arbitrary nature of the natural spectral-kinetic contours among the varying samples dictates that the residual weighting of the photoelectron count cannot be justifiably normalized or referenced to any one given peak (t,λ) channel coordinate or intensity integral to afford an absolutely equitable statistical weighting either within or among the images. This is obvious because if one arbitrarily chooses a peak channel or coordinate to normalize for one image one would necessarily use different residual weighting (based on the assumption that $\sigma^2 \cong M_i$) when comparing any other (t) or (λ) channel or (t,λ) coordinate channels or total integrated intensity, $T_{\mathrm{int}}(t,\lambda)$, of that or any other image. The robust L_1 method (Draper & Smith 1998) minimizes the sum of the absolute deviations and is defined as

$$L_1 = \sum_{i=1}^{N} |R_i|. \tag{B2}$$

The L_1 method assumes the residual error distribution is best defined by a Laplace distribution function (Evans *et al.* 1993), which has a sharper peak and more heavily populated tails than a normal distribution.

(c) Analyses of the randomness of the residual errors

The residual error distributions resulting from the χ^2_v and L_1 fits were comparatively analysed by constructing histograms comprising $N = 500$ bins each with a value of $(R_i = |0.0026|)$. The distributions were compared to the best fitting error distribution function (Evans *et al.* 1993) using a second χ^2-statistic,

$$\text{second } \chi^2 = \frac{1}{N - m - 1} \sum_{i=1}^{N} \left(\frac{(D_i - M_i)^2}{M_i} \right), \tag{B3}$$

where m represents the fitting parameters for the symmetrical error distribution function, defined as

$$y = \mathrm{AMP} \times \exp\left(-\frac{1}{2} \frac{|x - \mathrm{CTR}|^{(2/\mathrm{SHAPE})}}{\mathrm{WID}} \right), \tag{B4}$$

with the SHAPE parameter, that varies between 1 and 2, where 1 determines a Gaussian distribution and 2 determines a Laplace or double-exponential distribution. The SHAPE parameter was critical for evaluating these comparative analyses because the χ^2_v method assumes a Gaussian residual distribution whereas the robust L_1 method assumes a Laplace error distribution. The mode (CTR) of the error was fixed at 0 to test for symmetry about the ideal mean, while the WID, AMP and SHAPE parameters were free floating.

The randomness of the residual distribution about the assumed mean, $\bar{x} = 0$, was also determined using the Runs test as defined by Draper & Smith (1998). The Runs test analyses only the sign, and not the amplitude of the residual value, but was still a useful indicator of successful model minimization in these analyses. The number of consecutive signs or runs, in the residuals time-series for each λ channel was compared with the expected number of runs (and a standard deviation) that was determined by counting the number of positive and negative signs in each time-series and assuming a completely random sequence. Standard normal variates were then calculated for each time channel to test the assumptions that there were either too few ($|\mathcal{Z}_{\mathrm{tf}}|$) or too many ($|\mathcal{Z}_{\mathrm{tm}}|$) runs in the time-series compared with a completely random residual pattern. The global $\bar{x} \pm \sigma$ was then calculated for all wavelength channels and mean values of $|\mathcal{Z}_{\mathrm{tf}}|$ (or $|\mathcal{Z}_{\mathrm{tm}}|$) that were less than or equal to three standard deviations were accepted as a general 'rule of thumb' (Straume & Johnson 1992).

Additionally, each time-series for each wavelength channel was analysed for autocorrelation trends by use of the Durbin–Watson d-statistic (Draper & Smith 1998) and a global $d = \bar{x} \pm \sigma$ for all wavelength channels was calculated (Straume & Johnson 1992). It is generally accepted that values approaching the lowest theoretical value of $d = 0$ indicate positive serial correlations whereas values approaching the maximum theoretical $d = 4$ indicate negative serial correlations. Thus, the test of the null hypothesis for no autocorrelation was viewed 'qualitatively' as being meaningful if the $d = \bar{x} \pm \sigma$ range encompassed the natural mean of the d-statistic distribution that equals two.

REFERENCES

Adams III, W. W., Demmig-Adams, B., Winter, K. & Schreiber, U. 1990 The ratio of variable to maximum chlorophyll fluorescence from photosystem II, measured in leaves at ambient temperatures and at 77 K, as an indicator of the photon yield of photosynthesis. *Planta* **180**, 166–174.

Agati, G., Cerovic, Z. G. & Moya, I. 2000 The effect of decreasing temperature up to chilling values on the *in vivo* F_{685}/F_{735} chlorophyll fluorescence ratio in *Phaseolus vulgaris* and *Pisum sativum*. The role of photosystem I contribution to the 735 nm fluorescence band. *Photochem. Photobiol.* **72**, 75–84.

Alcala, J. R., Gratton, E. & Prendergrast, F. G. 1987 Resolvability of fluorescence lifetime distributions using phase fluorometry. *Biophys. J.* **51**, 587–596.

Baker, N. (ed.) 1996 *Photosynthesis and the environment*. Advances in photosynthesis research, vol. 5. Dordrecht, The Netherlands: Kluwer.

Bassi, R., Hinz, U. & Barbato, R. 1985 The role of the light harvesting complex and photosystem II in thylakoid stacking in the *chlorina*-f2 barley mutant. *Carlsberg Res. Commun.* **50**, 347–367.

Bevington, P. R. 1969 *Data reduction and error analysis for the physical sciences*. New York: McGraw-Hill.

Bossmann, B., Knoetzel, J. & Jansson S. 1997 Screening of *chlorina* mutants of barley (*Hordeum vulgare* L.) with antibodies against light-harvesting proteins of PS I and PS II: absence of specific antenna proteins. *Photosynth. Res.* **52**, 127–136.

Briantais, J.-M. 1994 Light-harvesting chlorophyll *a*–*b* complex requirement for regulation of photosystem II photochemistry by non-photochemical quenching. *Photosynth. Res.* **40**, 287–294.

Briantais, J.-M., Dacosta, J., Goulas, Y., Ducruet, J.-M. & Moya, I. 1996 Heat stress induces in leaves an increase of the minimum level of chlorophyll fluorescence, F_o: a time-resolved analysis. *Photosynth. Res.* **48**, 189–196.

Bühler, C. A., Graf, U., Hochstrasser, R. A. & Anliker, M. 1998 Multidimensional fluorescence spectroscopy using a streak camera based pulse fluorometer. *Rev. Sci. Instr.* **69**, 1512–1518.

Campillo, A. J. & Shapiro, S. L. 1983 Picosecond streak fluorometry—a review. *IEEE J. Quantum Elec.* **19**, 585–603.

Chow, W. S., Hope, A. B. & Anderson, J. M. 1991 Further studies on quantifying photosystem II in vivo by flash-induced oxygen yield from leaf discs. *Aust. J. Plant Physiol.* **18**, 397–410.

Davis, L. M. & Parigger, C. 1992 Use of a streak camera for time-resolved photon counting fluorimetry. *Meas. Sci. Technol.* **3**, 85–90.

Draper, N. R. & Smith, H. 1998 *Applied regression analysis*, 3rd edn. New York: Wiley.

Evans, M., Hastings, T. & Peacock, B. 1993 *Statistical distributions*, 2nd edn. New York: Wiley.

Falbel, T. G., Staehelin, A. & Adams III, W. W. 1994 Analysis of xanthophyll carotenoids and chlorophyll fluorescence in light intensity-dependent chlorophyll-deficient mutants of wheat and barley. *Photosynth. Res.* **42**, 191–202.

Falk, S., Krol, M., Maxwell, D. P., Rezansoff, D. A., Gray, G. R. & Huner, N. P. A. 1994 Changes in *in vivo* fluorescence quenching in rye and barley as a function of reduced PS II light harvesting antenna size. *Physiol. Plants* **91**, 551–558.

Frauenfelder, H. A., Parak, F. & Young, R. D. 1988 Conformational substates in proteins. *A. Rev. Biophys Biophys. Chem.* **17**, 451–479.

Genty, B., Wonders, J. & Baker, N. R. 1990 Non-photochemical quenching of F_o in leaves is emission wavelength dependent: consequences for quenching and its interpretation. *Photosynth. Res.* **26**, 133–139.

Gilmore, A. M. & Govindjee 1999 How higher plants respond to excess light: understanding energy dissipation strategies for photosystem II. In *Concepts in photobiology: photosynthesis and photomorphogenesis* (ed. G. S. Singhal, G. Renger, S. K. Sopory, K.-D. Irrgang & Govindjee), pp. 513–548. New Delhi, India: Narosa Publishing House.

Gilmore, A. M. & Yamamoto, H. Y. 1991 Resolution of lutein and zeaxanthin using a lightly carbon-loaded C18 high-performance liquid chromatographic column. *J. Chromatogr.* **543**, 137–145.

Gilmore, A. M., Hazlett, T. L., Debrunner, P. G. & Govindjee 1996 Photosystem II chlorophyll *a* fluorescence lifetimes are independent of the antenna size differences between barley wild-type and *chlorina* mutants: photochemical quenching and xanthophyll-cycle dependent nonphotochemical fluorescence quenching. *Photosynth. Res.* **48**, 171–187.

Gilmore, A. M., Shinkarev, V. P., Hazlett, T. L. & Govindjee 1998 Quantitative analysis of the effects of intrathylakoid pH and xanthophyll cycle pigments on the chlorophyll *a* fluorescence lifetime distributions and intensity in thylakoids. *Biochemistry* **37**, 13 582–13 593.

Govindjee 1995 Sixty-three years since Kautsky: chlorophyll *a* fluorescence. *Aust. J. Plant Physiol.* **22**, 131–160.

Govindjee & Yang, L. 1966 Structure of the red fluorescence band in chloroplasts. *J. Gen. Physiol.* **49**, 763–780.

Härtel, H. & Lokstein, L. 1995 Relationship between quenching of maximum and dark-level chlorophyll fluorescence *in vivo*: dependence on photosystem II antenna size. *Biochim. Biophys. Acta* **1228**, 91–94.

Haehnel, W., Nairn, J. A., Reisberg, P. & Sauer, K. 1982 Picosecond fluorescence kinetics and energy transfer in chloroplasts and algae. *Biochim. Biophys. Acta* **680**, 161–173.

Hodges, M. & Moya, I. 1986 Time-resolved chlorophyll fluorescence studies of photosynthetic membranes: resolution and characterization of four kinetic components. *Biochim. Biophys. Acta* **849**, 193–202.

Holcomb, C. T. & Knox, R. S. 1996 The relationship of intercompartmental excitation transfer rate constants to those of an underlying physical model. *Photosynth. Res.* **50**, 117–131.

Holzwarth, A. R. 1988 Time resolved chlorophyll fluorescence. In *Applications of chlorophyll fluorescence* (ed. H. K. Lichtenthaler), pp. 21–31. Dordrecht, The Netherlands: Kluwer.

Hungerford, G. & Birch, D. J. S. 1996 Single-photon timing detectors for fluorescence lifetime spectroscopy. *Meas. Sci. Technol.* **7**, 121–135.

Knoetzel, J. & Simpson, D. 1991 Expression and organisation of antenna proteins in the light- and temperature-sensitive barley mutant *chlorina* f104. *Planta* **185**, 111–123.

Knoetzel, J., Bossmann, B. & Grimme, H. 1998 *Chlorina* and *viridis* mutants of barley (*Hordeum vulgare* L.) allow assignment of long-wavelength chlorophyll forms to individual Lhca proteins of photosystem I *in vivo*. *FEBS Lett.* **436**, 339–342.

Knutson, J. R. 1992 Alternatives to consider in fluorescence decay analysis. *Meth. Enzymol.* **210**, 357–374.

Krause, G. H., Briantais, J.-M. & Vernotte, C. 1983 Characterization of chlorophyll fluorescence quenching in chloroplasts by fluorescence spectroscopy at 77 K. I. ΔpH-dependent quenching. *Biochim. Biophys. Acta* **723**, 169–175.

Krugh, B. W. & Miles, D. 1995 Energy transfer for low temperature fluorescence in PS II mutant thylakoids. *Photosynth. Res.* **44**, 117–125.

Lavorel, J. 1963 Indications d'ordre spectroscopique sur l'heterogeneité de la chlorophylle *in vivo*. *Colloques Internationaux de Centre National de la Recherche Scientifique* **119**, 161–176.

Li, X. P., Björkman, O., Shih, C., Grossman, A., Rosenquist, M., Jansson, S. & Niyogi, K. K. 2000 A pigment-binding protein essential for regulation of photosynthetic light harvesting. *Nature* **403**, 391–395.

Lin, S. & Knox, R. S. 1988 Time resolution of a short-wavelength chloroplast fluorescence component at low temperature. *J. Luminescence* **40–41**, 209–210.

Melkozernov, A. N., Schmid, V. H. R., Schmidt, G. W. & Blankenship, R. E. 1998 Energy redistribution in heterodimeric light-harvesting complex LHC I-730 of photosystem I. *J. Phys. Chem.* **102**, 8183–8189.

Mimuro, M., Yamazaki, I., Tamai, N. & Katoh, T. 1989 Excitation energy transfer in phycobilisomes at −196 °C isolated from the cyanobacterium *Anabaena variabilis* (M-3): evidence for the plural transfer pathways to the terminal emitters. *Biochim. Biophys. Acta* **973**, 153–162.

Pearlstein, R. M. 1982 Exciton migration and trapping in photosynthesis. *Photochem. Photobiol.* **35**, 835–844.

Pfündel, E. 1998 Estimating the contribution of photosystem I to total leaf chlorophyll fluorescence. *Photosynth. Res.* **56**, 185–195.

Porra, R. J., Thompson, W. A. & Kriedemann, P. E. 1989 Determination of accurate extinction coefficients and simultaneous equations for assaying chlorophyll *a* and *b* with four different solvents: verification of the concentration of chlorophyll by atomic absorption spectroscopy. *Biochim. Biophys. Acta* **975**, 384–394.

Roelofs, T. A., Lee, C.-H. & Holzwarth, A. R. 1992 Global target analysis of picosecond chlorophyll fluorescence kinetics from peas chloroplasts. *Biophys. J.* **61**, 1147–1163.

Rundel, R. 1991 *Technical guide to peak fit, nonlinear curve-fitting software*. Corte Madera, CA: Jandel Scientific.

Schiller, N. H. & Alfano, R. R. 1980 Picosecond characteristics of a spectrograph measured by a streak camera/video readout system. *Optics Comm.* **35**, 451–454.

Schmuck, G. & Moya, I. 1994 Time-resolved chlorophyll fluorescence spectra of intact leaves. *Remote Sens. Environ.* **47**, 72–76.

Schreiber, U., Klughammer, C. & Neubauer, C. 1988 Measuring P700 absorbance changes around 830 nm with a new type of pulse modulation system. *Z. Naturforsch.* **43c**, 686–698.

Simpson, D. J., Machold, O., Höyer-Hansen, G. & Von Wettstein, D. 1985 Chlorina mutants of barley (*Hordeum vulgare* L.). *Carlsberg Res. Commun.* **50**, 223–238.

Singhal, G. S., Renger, G., Sopory, S. K., Irrgang, K.-D. & Govindjee (eds) 1999 *Concepts in photobiology. Photosynthesis and photomorphogenesis*. New Delhi, India: Narosa Publishing House.

Straume, M. & Johnson, M. L. 1992 Analysis of residuals: criteria for determining goodness-of-fit. *Meth. Enzymol.* **210**, 87–105.

Tsuchiya, Y. 1984 Advances in streak camera instrumentation for the study of biological and physical processes. *IEEE J. Quantum Elec.* **20**, 1516–1528.

Van Kooten, O. & Snel, J. F. H. 1990 The use of fluorescence nomenclature in plant stress physiology. *Photosynth. Res.* **25**, 147–150.

Weis, E. 1985 Chlorophyll fluorescence at 77 K in intact leaves: characterization of a technique to eliminate artifacts related to self-absorption. *Photosynth. Res.* **6**, 73–86.

Yamazaki, I., Mimuro, M., Murao, T., Yamazaki, T., Yoshihara, K. & Fujita, Y. 1984 Excitation energy transfer in the light harvesting antenna system of the red alga *Porphyridium cruentum* and the blue-green alga *Anacystis nidulans*: analysis of time-resolved fluorescence spectra. *Photochem. Photobiol.* **39**, 233–240.

Discussion

H. Y. Yamamoto (*Department of Plant Molecular Physiology, University of Hawaii, USA*). What constitutes a saturating concentration of zeaxanthin or anthereaxanthin (or lutein) with respect to the non-photochemical quenching activity of PS II?

A. M. Gilmore. Aside from minor changes associated with pleiotropic effects, as may be observed in some of the xanthophyll mutants of *Arabidopsis*, one can generally predict given a saturating level of thylakoid lumen acidification that as little as 2 or 3 mols of the xanthophylls zeaxanthin or antheraxanthin per PS II will be saturating.

H. Y. Yamamoto. If 2 or 3 mols of xanthophylls are sufficient to saturate the PS II non-photochemical quenching activity then why do plants tend to accumulate more xanthophylls and why do they then need to undergo de-epoxidation at all?

A. M. Gilmore. It is my point of view that much like pollen generation, plants naturally tend to overcompensate for this particular biosynthetic pathway. The analogy is very clear because it only takes one xanthophyll to quench one PS II unit and it only takes one pollen grain to fertilize and ovum to make a seed, yet plants tend to make an enormous excess of pollen that is usually simply lost in the wind. It is quite curious that no-one ever ascribes a profound significance to the natural tendency to generate excess pollen whereas I have been asked this question regarding the xanthophyll cycle many times.

E. Hideg (*Institute of Plant Biology, Biological Research Center, Szeged, Hungary*). Please comment on the physiology of *Mantoniella squamata*, is it grown under special light conditions?

A. M. Gilmore. We grow *M. squamata* under about 60 μmol photons $m^{-2} s^{-1}$. However, our actinic light treatments were usually up to 1000 μmol photons $m^{-2} s^{-1}$ for as long as 15 min. After the end of the light treatment we observed little if any irreversible quenching of PS II fluorescence that we could use or interpret as an indicator of photoinhibition.

E. Hideg. Is it light sensitive as compared to other algae?

A. M. Gilmore. I would conclude that in the short term, as pertains to the experiments presented in the Discussion Meeting but not reported here, *M. squamata* is not extremely or obviously more light sensitive than other algae I have worked with including diatoms and *Chlamydomonas* grown under similar light conditions, i.e. 60 to 100 μmol photons $m^{-2} s^{-1}$.

E. Garcia-Mendoza (*Department of Microbiology, University of Amsterdam, The Netherlands*). What controls the flip flop of antheraxanthin in *Mantoniella squamata*?

A. M. Gilmore. My hypothetical interpretation is that in the presence of lumen acidification, with the PS II inner antennae proteins protonated, the antheraxanthin molecule binds to the transmembrane proteins more tightly (in the position where its de-epoxidized end-group faces the lumen), than does the violaxanthin molecule. Thus antheraxanthin rarely and almost never flips to form zeaxanthin with a pH gradient.

E. Garcia-Mendoza. What about epoxidation characteristics?

A. M. Gilmore. My hypothesis is that when the lumen acidity is neutralized in the dark, antheraxanthin binding is less efficient and the molecule is free to flip in the membrane to interact with the epoxidase enzyme on the stroma side. Hence it is the protonation of the proteins by the pH gradient that causes antheraxanthin to stop flipping, and this inhibits its conversion to zeaxanthin. Likewise, without the pH gradient antheraxanthin converts back to violaxanthin with similar kinetics as seen in higher plant leaves or chloroplasts.

Note added in proof. Agati *et al.* (2000) independently showed that the F_{735} band emitted from the PS I antenna compartment exhibits a much shorter fluorescence lifetime than F_{685} from PS II in leaves. The influence of F_{735} on the average fluorescence lifetime is most strongly exhibited under the F_o conditions when PS II photochemistry is at a maximum.

PHILOSOPHICAL TRANSACTIONS OF THE ROYAL SOCIETY B BIOLOGICAL SCIENCES